Review of Scientific Instruments

A simplified and versatile calibration method for multi-camera optical systems in 3D particle imaging

Cite as: Rev. Sci. Instrum. **90**, 035112 (2019); https://doi.org/10.1063/1.5080743
Submitted: 11 November 2018 . Accepted: 28 February 2019 . Published Online: 22 March 2019

N. Machicoane, A. Aliseda, R. Volk, and M. Bourgoin

Review of Scientific Instruments ARTICLE scitation.org/journal/rsi

A simplified and versatile calibration method for multi-camera optical systems in 3D particle imaging

Cite as: Rev. Sci. Instrum. 90, 035112 (2019); doi: 10.1063/1.5080743
Submitted: 11 November 2018 • Accepted: 28 February 2019 •
Published Online: 22 March 2019

N. Machicoane,[1,a] A. Aliseda,[1] R. Volk,[2] and M. Bourgoin[2]

AFFILIATIONS

[1] Department of Mechanical Engineering, University of Washington, Seattle, Washington 98195, USA
[2] University of Lyon, ENS de Lyon, Université Claude Bernard, CNRS, Laboratoire de Physique, F-69342 Lyon, France

[a] Electronic mail: nathanael.machicoane@ens-lyon.org

ABSTRACT

This article describes a stereoscopic multi-camera calibration method that does not require any optical model. It is based on a measure of the light propagation within the measurement volume only instead of modeling its entire path up to the sensors. The calibration uses simple plane by plane transformations which allow us to directly link pixel coordinates to light rays. The appeal of the proposed method relies on the combination of its simplicity of implementation (it is particularly easy to apply in any sophisticated optical imaging setup), its versatility (it can easily handle index-of-refraction gradients, as well as complex optical arrangements), and its accuracy {we show that the proposed method gives better accuracy than commonly used techniques, based on Tsai's simple pinhole camera model [R. Tsai, J. Rob. Autom. **3**, 323 (1987)], while its numerical implementation remains extremely simple}. Based on ideas that have been available in the fluid mechanics community, this method is a compact turn-key algorithm that can be implemented with open-source routines.

I. INTRODUCTION

Flow velocity measurements, based on the analysis of the motion of particles imaged with digital cameras, have become the most commonly used metrology technique in contemporary fluid mechanics research.[1,2] *Particle Image Velocimetry* (PIV) and *Particle Tracking Velocimetry* (PTV) are two widely used methods that enable the characterization of a flow from an Eulerian (PIV) or Lagrangian (PTV) point of view. Additionally, particle imaging is used in image correlation techniques that provide strain or strain rate measurements,[3,4] and PTV can yields information about a dispersed phased carried by the flow.[5–8] Several aspects influence the accuracy and reliability of the measurements obtained with these techniques:[9] resolution (temporal and spatial), dynamical range (spatial and temporal), capacity to measure 2D or 3D components of velocity in a 2D or 3D domain, or statistical convergence. These imaging and analysis considerations depend not only on the hardware (camera resolution, repetition rate, on board memory, or optical system) but also on the software (optical calibration, particle identification and tracking algorithms, image correlations, or dynamical post-processing) used in the measurements.

In the context of particle tracking with applications in fluid mechanics, particle center detection and tracking algorithms have been the focus of more studies[10,11,22] than optical calibration and 3D position determination. Although many strategies with various degrees of complexity have been developed for camera calibration,[12–17] most existing experimental implementations of multi-camera particle tracking use the pinhole camera model, originally proposed by Tsai in 1987[18] as the basis for calibration (sketched in Fig. 1).[13] Tsai's model requires non-linear elements to account for each aspect of the optical path. In practice, realistic experimental setups are either complex or time-consuming to model via individual optical elements in the Tsai method or are over-simplified by ignoring certain elements such as windows or compound lenses, with loss of accuracy.

This article describes a new camera calibration method that can be more accurate than a simple Tsai model in terms of absolute 3D stereo-positioning of particles, while easily handling any of the complexity or non-linearity in the optical setup described above. The key point of the method is that, instead of defining an optical model of the imaging system, it defines, without any physical *a priori* model, a transformation that connects each point in the camera sensor to

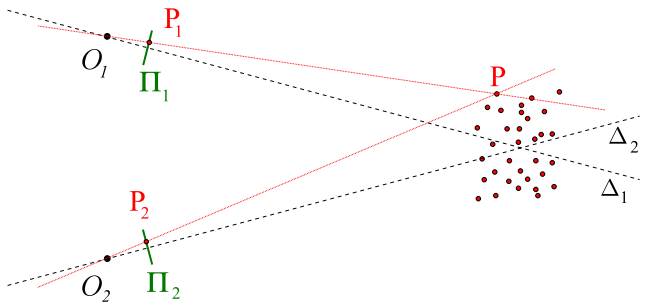

FIG. 1. Sketch of Tsai's pinhole camera model and stereo-matching: the position of a particle in the real world corresponds to the intersection of 2 lines Δ_1 and Δ_2, each emitted by the camera centers O_1 and O_2 and passing through the position of particles P_1 and P_2 detected on a each camera plane Π_1 and Π_2.

the actual light beam across the measurement volume. This transformation contains the necessary degrees of freedom but does not require any operator input beyond a set of calibration images taken across the measurement volume (typical of any 3D calibration process). The multi-camera calibration proposed can be applied to other 3D imaging setups such as tomographic PIV or PTV.

II. CALIBRATION PRINCIPLE

3D particle imaging methods require an appropriate calibration method to perform the stereo-matching between the several sets of 2D positions of particles in the *pixel coordinate system* for each camera and the absolute 3D position of the particles in the *real-world coordinate system*. The accuracy of the calibration method directly impacts the accuracy of the 3D positioning of the particles in the real world.

The calibration method proposed here is based on the simple idea that no matter how distorted a recorded image is, each bright point on the pixel array is associated with the ray of light that produced it, such that the corresponding light source (typically a scattering particle) can lie anywhere on this ray of light. An appropriate calibration method should be able to directly attribute to a given doublet (x_p, y_p) of pixel coordinates the corresponding ray path. If the index of refraction in the measurement volume of interest is uniform (so that light propagates along a straight line inside the measurement volume), each doublet can be associated with a straight line Δ (defined by 6 parameters in 3D: one point O_Δ and one vector $\vec{V}_\Delta$), regardless of the path outside the volume of interest, which can be very complex as material interfaces and lenses are traversed. The method consists in building a *pixel-to-line* transformation $\mathcal{I}$ to perform this correspondence between pixel coordinates and each of the 6 parameters of the ray of light: $(x_p, y_p) \xrightarrow{\mathcal{I}} (O_\Delta, \vec{V}_\Delta)$. Note that in the experimental demonstration of the methods proposed here, it is assumed that light propagates in a straight line as the medium in the experiment presented is homogeneous, but, as discussed below, it is trivial to extend the method to handle curved light path.

While the proposed method can seem similar to the Tsai approach, since it also builds a ray of light for each doublet, there is a significant difference in that Tsai's approach which assumes a physical model for the camera and optical path, with few parameters and the constraint that all rays must pass through the optical center. The quality of the inferred transformation will therefore be sensitive to variations of the setup leading to calibration data which may no longer match the model due to optical distortions, imperfect interfaces, sophisticated optical arrangements (such as a tilt-and-shift lens), and other possible complexities. Handling such complexities in pinhole-like models is doable but generally requires specific modifications of the underlying model (implying generally complex algorithms, difficult at least for non-experts). The present approach, based on empirical transformations from the actual calibration data, embeds an arbitrary number (as described below) of parameters that are not related to any physical property of the optical system. The calibration, therefore, self-adapts to optical imperfections, media inhomogeneities (outside of the measurement volume), or complex lens arrangements. Additionally, the generalization of the method to cases where light does not propagate in a straight line is straightforward: it is sufficient to build the transformation $\mathcal{I}$ with the parameters required to describe the expected curved path of light in the medium of interest (for instance, a parabola in a linearly stratified medium or an arbitrary higher order polynomial for more complex situations).

III. PRACTICAL IMPLEMENTATION

An implementation of the method is proposed where the *pixel-to-line* transformation $\mathcal{I}$ is built as an interpolant from experimental images of a calibration target with known patterns at known positions. The open-source routines described below are provided in the supplementary material. The process is described for one camera only for clarity's sake.

A calibration target consisting in a grid of equally separated dots is moved perpendicularly to its plane (along the OZ axis) using a micrometric screw, being imaged at several known Z positions by all cameras. Note that micrometric translation of planes is not *a priori* required, and a set of images of points with known location, in arbitrary planes, can very well be used instead. Also, with minor changes, other planar patterns than points (such as a checkboard pattern) can also be used. In total, N_Z plane images are taken with each camera: I_j is the calibration image when the plane is at position Z_j (with $j \in [1, N_Z]$). For the purpose of testing, the quality of the calibration method and its sensitivity to the number of planes used, up to $N_Z = 13$ planes, were collected across the measurement volume. The calibration protocol, sketched in Fig. 2, then proceeds as follows:

1. **Dot center finding**. For each calibration image I_j, the dot centers are detected, giving a set $(x_j^k, y_j^k)_{k\in[1;N_j]}$ of pixel coordinates. N_j is the number of dots actually detected on each image I_j. *Real-world* coordinates of the dots $(X_j^k, Y_j^k, Z_j^k)_{k\in[1;N_j]}$ are known. Lowercase coordinates represent *pixel coordinates*, while uppercase coordinates represent *absolute real-world coordinates*.
2. **2D plane-by-plane transformations**. For each position Z_j of the calibration target, the measured 2D pixel coordinates $(x_j^k, y_j^k)_{k\in[1;N_j]}$ and the known 2D real-world coordinates $(X_j^k, Y_j^k)_{k\in[1;N_j]}$ are used to infer a spatial transformation $\mathcal{T}_j$ projecting 2D pixel coordinates onto 2D real-world coordinates in the plane XOY at position Z_j. Different types of

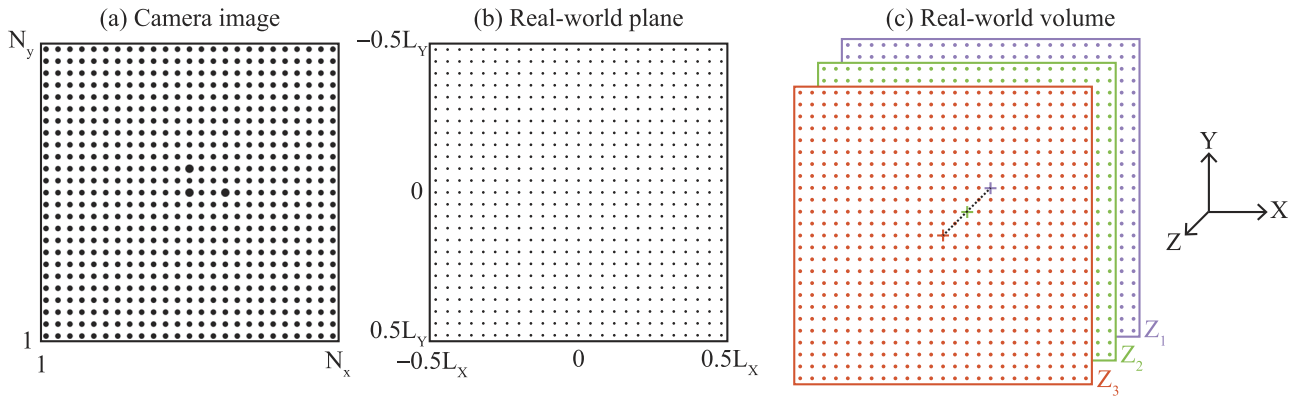

FIG. 2. Sketch of the calibration method. (a) Calibration target imaged on one plane, over $N_x \times N_y$ pixels. (b) Same plane transformed into real-world coordinates on the domain $L_X \times L_Y$ (no optical distortion is considered here for simplicity so the transformation is linear in the 2D plane). (c) Stacks of planes in 3D real-world coordinates. Dots at (X, Y) are fitted along Z_i, $1 \le i \le N_Z$ to build the interpolant $\mathcal{I}$. For simplicity, only 3 planes are considered here with the 3 dots identified as crosses and a linear fit is used (dashed line). Note that the fit is only done within the calibration volume where the target is translated along the N_z planes and does not extend to the cameras.

transformations can be inferred from a simple linear projective transformation to high order polynomial transformations if non-linear optical aberrations need to be corrected (common optical aberrations are adequately captured by a 3rd order polynomial transformation). This is a standard planar calibration procedure, where an estimate of the accuracy of the 2D plane-by-plane transformation can be obtained from the distance, in pixel coordinates, between $(x_j^k, y_j^k)_{k\in[1;N_j]}$ and $\mathcal{T}_j^{-1}\left(X_j^k, Y_j^k, Z_j\right)_{k\in[1;N_j]}$. The maximum error for the images used here is less than 2 pixels.

3. **Building the pixel-line interpolant**. The key step in the calibration method builds the pixel-line interpolant, $\mathcal{I}$, which directly connects pixels coordinates to a ray path. To achieve this, a grid of $N_\mathcal{I}$ interpolating points in pixel coordinates $(x_l^\mathcal{I}, y_l^\mathcal{I})_{l\in[1,N_\mathcal{I}]}$ is defined, for which the ray paths have to be computed. The inverse transformations $\mathcal{T}_j^{-1}$ are used to project each point of this set back onto the real-world planes (X, Y, Z_j), for each of the N_Z positions Z_j. Each interpolating point $(x_l^\mathcal{I}, y_l^\mathcal{I})$ is therefore associated with a set of N_Z points in the real world $(X_l^\mathcal{I}, Y_l^\mathcal{I}, Z_j)$. Conversely, these points in the real world can be seen as a discrete sampling of the ray path which impacts the sensor of the camera at $(x_l^\mathcal{I}, y_l^\mathcal{I})$. If light propagates as a straight line, the N_Z points $(X_l^\mathcal{I}, Y_l^\mathcal{I}, Z_j)$ should be aligned. By a simple linear fit of these points, each interpolating point $(x_l^\mathcal{I}, y_l^\mathcal{I})$ is related to a line Δ_l, defined by a point $O_{\Delta_l} = (X_l^0, Y_l^0, Z_l^0)$ and a vector $\vec{V}_{\Delta_l} = (Vx_l, Vy_l, Vz_l)$ (hence 6 parameters for each interpolating point). Each of these rays from the $N_\mathcal{I}$ interpolation points is used to compute the interpolant $\mathcal{I}$, which allows any pixel coordinate (x, y) in the camera to be connected to its ray path $(O_\Delta, \vec{V}_\Delta)$ corresponding to all possible positions of light sources that could produce a bright spot in (x, y). Finding the 3D position of a point (or particle) can be done by finding the location of crossing of all the rays coming from the different cameras. All pixels in each camera were chosen here to build the interpolant as this step is done only once, but the method can be applied with a sub-sampled pixel array. Alternatively, one can also choose not to build the interpolant but to apply the plane-by-plane transformations and the polynomial fit leading to the light ray directly from the actual data (for instance, corresponding to detected centers of particle images).

IV. COMPARISON WITH THE TSAI METHOD

The calibration procedure proposed by Tsai[18] has been widely used to recover the optical characteristics of an imaging system and reconstruct the 3D position of an object. The accuracy of the proposed imaging calibration procedure is assessed by comparing it with a simple Tsai implementation. Given the simplicity of implementation of the proposed method, we consider for the present comparison a simple version of the Tsai model, accounting only for cubic radial distortion. While improved optical elements modeling in the Tsai model could increase the accuracy, they come at an increased user workload.

The stereoscopic optical arrangement is sketched in Fig. 3. It aims at performing particle tracking velocimetry in a 1 cm-thick laser sheet near the geometrical center of a turbulent water flow created in an icosahedron [the Lagrangian Exploration Module (LEM) flow; see Refs. 19, 20, and 23 for more details]. Each camera objective, nearly perpendicular to its corresponding window, is mounted in the Scheimpflug configuration[21] so that all particles present in the laser sheet are nearly in focus independently of their position in the field of view. To perform both calibrations, we used a translucent plate mounted parallel to the laser sheet with dots size equal to 2 mm. These points were equally spaced by a distance of 5 mm in both directions, and the thickness of the plate was approximately 0.2 mm. This plate was attached to a manual micro-metric traverse that was able to give displacements with an accuracy of the order of 10 μm. For both methods, up to 13 images of the target were used, spaced 1 mm from each other along the Z axis. The interpolant for the proposed method was built considering a simple line equation for light propagation as light is expected to propagate straight in the homogeneous medium we considered.

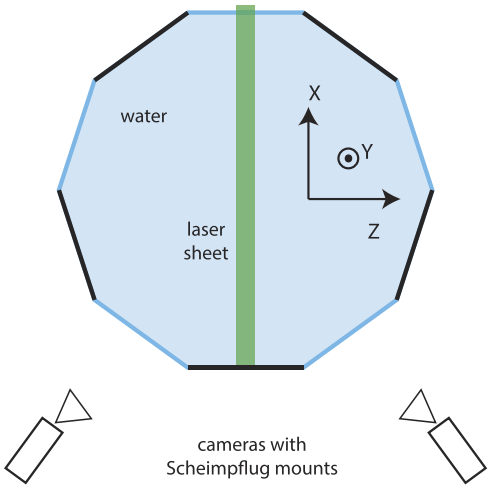

FIG. 3. Top view of the stereoscopic optical arrangement used for particle tracking in the LEM flow. Both cameras use an objective with Scheimpflug mount so that all objects in a $10 \times 10 \times 1$ cm^3 region near the geometrical center are approximately in focus on the camera sensor. The calibration mask is placed parallel to the laser sheet and moved in the Z direction.

TABLE I. Absolute deviation from the expected position of the targets averaged over space.

	d_X (μm)	d_Y (μm)	d_Z (μm)	d (μm)
Proposed calibration	32.7	12.6	39.2	59
Tsai model	121	171.1	112.7	266.6

The calibration methods use the 2D positions of the target dots and provide a series of positions that cannot match exactly the 3D real coordinates because, in both methods, the model parameters are obtained by solving an over-constrained linear system in the least-square sense. The calibration error, i.e., the absolute difference between the (known) real coordinates and the transformed ones, is computed to evaluate the calibration accuracy. This error can be estimated along each direction, e.g., d_X, or as a norm: $d = \sqrt{d_X^2 + d_Y^2 + d_Z^2}$ (Table I). Figure 4 plots the total 3D error averaged on the 13 planes used, for both the proposed method and the Tsai model.

The accuracy of the proposed calibration is superior to the simple Tsai one. The error is at least 300% smaller (depending on which component is considered) and is reduced to barely 0.5 pixel. It is important to note that the error map obtained with the Tsai method [Fig. 4(b)] seems to display a large bias along Y that could be due to the use of Scheimpflug mounts, which are typically not included in this Tsai calibration, and to the angle between the cameras and the tank windows. This hypothesis was verified by comparing the two calibration procedures in more conventional conditions (without the Scheimpflug mount and in air in order to avoid intermediate interfaces), where they give similar results with very small error. This also points out that, beyond its accuracy and simplicity of implementation, the proposed calibration method is highly versatile and can be used without modification and without loss of accuracy both in simple optical situations and in complex arrangements.

For the present optical arrangement and the new calibration method, the error in the Y positioning is smallest. Indeed, due to the shape of the experiment (an icosahedron), the y axis of the camera sensor is almost aligned with the Y direction so that this coordinate is fully redundant between the cameras, while the x axis of each camera sensor forms an angle $\alpha \simeq \pi/3$ with the X direction so that the accuracy on X positioning is lower. This directly impacts the accuracy on the Z positioning whose error is almost equal to the X positioning error.

V. DISCUSSION

Up to 13 planes were used to build the operator that yields the camera calibration. While two planes are the minimum required for the method, a larger number of planes imaged provide better accuracy. In this case study, the major sources of optical distortion were Scheimpflug mounts, imperfect lenses, and non-perpendicular interfaces. 7 planes provided an optimal trade-off between high accuracy and simplicity, with an error only 2% larger than with 13 planes, while using 3 planes yields an error 10% larger. If dealing with a more complex experiment, e.g., with a refraction index gradient, increasing the number of planes in the calibration would improve the results allowing the calibration operator to accurately capture the curvature of the light rays. On the contrary, for simpler situations (without interfaces and without Scheimpflug mounts), fewer planes would be required to achieve the same level of accuracy. As a matter of fact, the number of planes used impacts directly the effective number of hidden parameters in the calibration model and largely determine its accuracy. The 3rd order polynomial plane-by-plane transformations used here embed 10 parameters

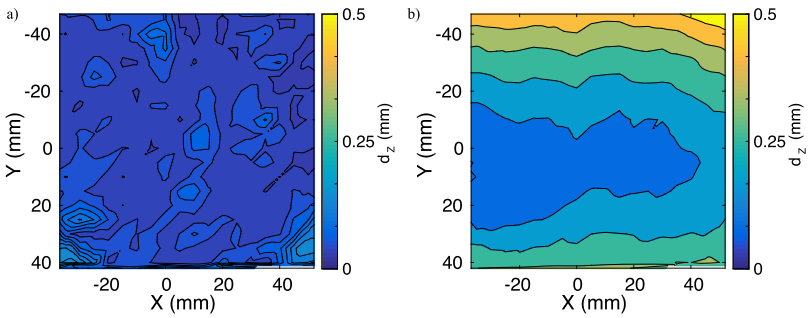

FIG. 4. Calibration error averaged over Z using the proposed calibration method (a) or Tsai model (b).

each (corresponding to the polynomial coefficients). The total number of effective degrees of freedom for the total calibration using N_z planes is, then, $N_p = 10N_z$. The simple Tsai model accounts only for radial distortions and thus typically embeds only on the order of 10 parameters. Taking this higher number of degrees of freedom into account, the improved accuracy of the proposed method compared to the Tsai model is somehow expected (as using 7 planes leads to a calibration model embedding 70 parameters). The present comparison may, thus, seem unfair to the Tsai model, but the basis for it was similar ease of implementation and not similar number of degrees of freedom. One can consider more sophisticated pinhole camera models, with additional parameters properly accounting for tilt and shift corrections, up to a point where they would match the accuracy reached with the proposed calibration here, but with much more effort from the user in formulating the complex optical model. This is because such extensions of the pinhole approach are based on sophisticated physical and geometrical models, with algorithms which tend to be tedious to implement. A big advantage of the present calibration is its versatility and ease of algorithmic implementation, which remains identical (without loss of accuracy), irrespective of the optical path complexity.

The proposed calibration method has several advantages that make it worth implementing in a multi-camera particle imaging setup. First, it requires no model or assumption about the properties of the optical path followed by the light in the different media outside the volume of interest. The method computes a transformation that directly determines the equation for propagation of light in space (within the volume of interest). This ray equation is fully determined by the N_z plane-by-plane transformations. Second, this method is turnkey for any typical optical system. The implementation of the new method is easily done and can be used retroactively using previous calibration images.

To conclude, the calibration method proposed combines simplicity of implementation, versatility of application, and accuracy. The calibration algorithm and the operator calculation to convert pixel locations to physical locations, with minimal errors, are open-source and given in the the supplementary material but can easily be programmed in any language available to experimentalists. The new method is at least equally, and frequently more, accurate than the commonly used Tsai model, and it can be used more easily and in a wider range of optical configurations. As experimental setups get more complicated with more optical and light refraction elements, this method should prove simpler to implement and more accurate than approaches based on camera models.

SUPPLEMENTARY MATERIAL

The supplementary material contains the calibration algorithm, as well as examples for the plane-by-plane transform, interpolant computation, and resulting error estimation that can be tested on the user data or with the provided demo data for testing purposes.

ACKNOWLEDGMENTS

The authors would like to acknowledge the financial support of the European EUHIT I^3 project (Contract No. 312778), Labex TEC 21 (Contract No. ANR-11-LABX-0030), PALSE/2013/26, and IDEXLyon (Contract No. ANR-16-IDEX-0005) under the University of Lyon auspices.

REFERENCES

[1] R. J. Adrian, Annu. Rev. Fluid Mech. **23**, 261 (1991).
[2] *Springer Handbook of Experimental Fluid Dynamics*, edited by C. Tropea, A. Yarin, and J. F. Foss (Springer-Verlag, Berlin-Heidelberg, 2007).
[3] J. C. del Alamo, R. Meili, B. Alonso-Latorre, J. Rodriguez-Rodriguez, A. Aliseda, R. A. Firtel, and J. C. Lasheras, Proc. Natl. Acad. Sci. U. S. A. **104**(33), 13343–13348 (2007).
[4] J. Rodriguez-Rodriguez, C. Marugan-Cruz, A. Aliseda, and J. C. Lasheras, Exp. Therm. Fluid Sci. **35**, 301–310 (2011).
[5] Y. Sato and K. Yamamoto, J. Fluid Mech. **175**, 183–199 (1987).
[6] M. Virant and T. Dracos, Meas. Sci. Technol. **8**(12), 1539–1552 (1997).
[7] G. A. Voth, A. L. Porta, A. Crawford, J. Alexander, and E. Bodenschatz, J. Fluid Mech. **469**, 121 (2002).
[8] F. Toschi and E. Bodenschatz, Annu. Rev. Fluid Mech. **41**, 375–404 (2009).
[9] *Springer Handbook of Experimental Fluid Dynamics*, edited by C. Tropea, A. Yarin, and J. Foss (Springer-Verlag, Berlin, 2007), pp. 789–799.
[10] N. Ouellette, H. Xu, and E. Bodenschatz, Exp. Fluids **40**, 301 (2006).
[11] H. Xu, Meas. Sci. Technol. **19**, 075105 (2008).
[12] R. Y. Tsai and R. K. Lenz, "Real time versatile robotics hand/eye calibration using 3D machine vision," in *1988 IEEE International Conference on Robotics and Automation* (IEEE, 1988).
[13] J. Weng, P. Cohen, and M. Herniou, IEEE Trans. Pattern Anal. Mach. Intell. **14**, 965–980 (1992).
[14] J. Heikkila and O. Silven, in *Proceedings of IEEE Computer Society Conference on Computer Vision and Pattern Recognition* (IEEE, 1997).
[15] Z. Zhang, IEEE Trans. Pattern Anal. Mach. Intell. **22**(11), 1330–1334 (2000).
[16] D. Claus and A. W. Fitzgibbon, in *Proceedings of IEEE Computer Society Conference on Computer Vision and Pattern Recognition* (IEEE, 2005), pp. 213–219.
[17] F. Remondino and C. Fraser, in *ISPRS Commission V Symposium on Image Engineering and Vision Metrology* (WG, 2006), Vol. 36, No. 5, pp. 266–272.
[18] R. Tsai, IEEE J. Rob. Autom. **3**, 323 (1987).
[19] L. Fiabane, R. Zimmermann, R. Volk, J.-F. Pinton, and M. Bourgoin, Phys. Rev. E **86**, 035301 (2012).
[20] R. Zimmermann, Y. Gasteuil, M. Bourgoin, R. Volk, A. Pumir, and J.-F. Pinton, Rev. Sci. Instrum. **82**, 033906 (2011).
[21] A. Prasad and K. Jensen, Appl. Opt. **34**(30), 7092–7099 (1995).
[22] A. Clark, N. Machicoane, and A. Aliseda, Meas. Sci. Technol. **30**(4), 045302 (2019).
[23] N. Machicoane, M. López-Caballero, M. Bourgoin, A. Aliseda, and R. Volk, Meas. Sci. Technol. **28**(10), 107002 (2017).